Supporting Information

Insulator-quantum Hall transition in monolayer epitaxial graphene

Lung-I Huang[ab], Yanfei Yang[ac], Randolph E. Elmquist[a],
Shun-Tsung Lo[*d], Fan-Hung Liu[d], and Chi-Te Liang[*bde]

[a]*National Institute of Standards and Technology (NIST), Gaithersburg, MD 20899, USA*
[b]*Department of Physics, National Taiwan University, Taipei 106, Taiwan*
[c]*Department of Physics, Georgetown University, Washington, DC 20057, USA*
[d]*Graduate Institute of Applied Physics, National Taiwan University, Taipei 106, Taiwan*
[e]Geballe Laboratory for Advanced Materials (GLAM), Stanford University, Stanford, CA 94305, USA

*shuntsunglo@mail.ncku.edu.tw and ctliang@phys.ntu.edu.tw

Sample preparation and measurements

Epitaxial graphene (EG) is formed after decomposition and Si sublimation on the surface of SiC at high temperatures. Angle-resolved photoelectron spectroscopy shows that newly-grown samples measured *in situ* have carrier concentrations $n \approx 10^{13}$ cm^{-2}, ascribed to charge-transfer from an insulating graphene-like buffer layer that is covalently bonded to the SiC substrate.[1] In order to study the electronic transport with $|n| < 10^{12}$ cm^{-2}, electrostatic[2, 3] or photochemical[4] gating through an insulating dielectric, molecular doping[5] directly on the EG surface, or atomic intercalation[1, 6] beneath the buffer layer have been used to modify the carrier concentration. In order to achieve low density EG, Our EG devices were fabricated utilizing a clean lithography process[7] that leaves the surface free of resist residues. After this fabrication process doping occurs due to or initiated by chemical etching of the protective layer and exposure to air, producing typical carrier densities of order $n \approx 10^{11}$ cm^{-2}. The devices can be cycled to higher or lower carrier density repeatedly by annealing at 70 °C to 150 °C or by air exposure, implicating oxygen and water molecules from the air as the source of p-type molecular doping.[8, 9]

Longitudinal resistivity ρ_{xx} was obtained by averaging the data from both sides of the conducting channel [voltage probes 1, 3 and voltage probes 1* and 3*] and Hall resistivity ρ_{xy} was measured across the central pair [2 and 2*] of device contacts [Fig. S1]. In graphene as well as in heterostructures, low carrier concentrations are often associated with percolating current paths that mix ρ_{xx} with ρ_{xy}. Data measured at both directions of the magnetic field were combined based on the recognized symmetries of the resistivity components to eliminate this mixing [10], which is strong in highly disordered samples for large values of ρ_{xx}.

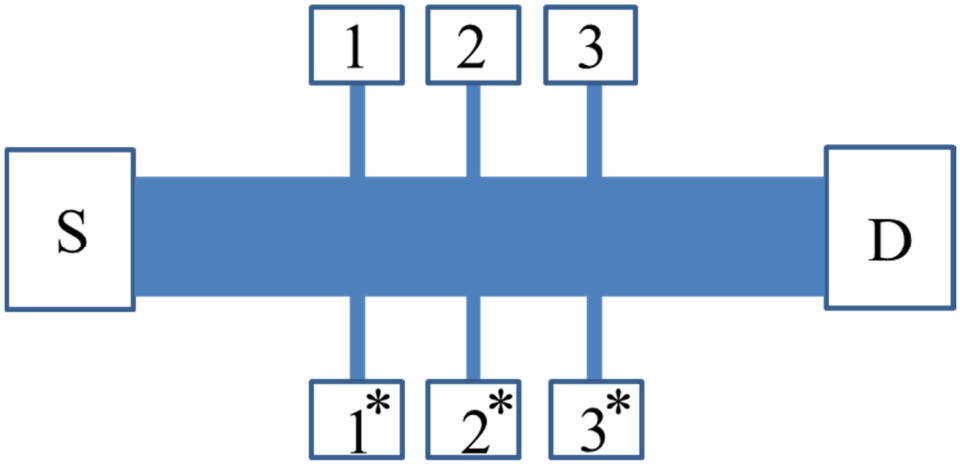

Figure S1 Schematic diagram showing a typical monolayer epitaxial graphene (EG) sample. S and D correspond to source and drain contacts. 1, 2, 3, 1^*, 2^* and 3^* are voltage probes. Channel dimensions, which are the same for all devices studied, are L = 0.6 mm, W = 0.1 mm, with voltage contacts spaced 0.1 mm apart along both sides of the device.

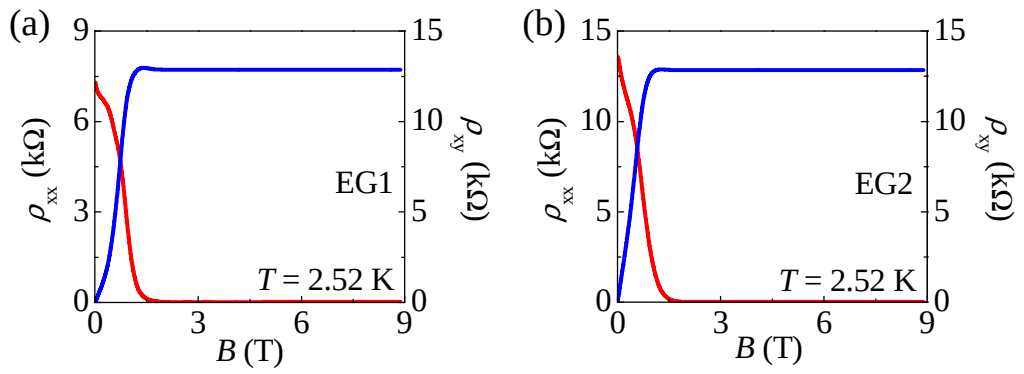

Figure S2. Resistivity values $\rho_{xx}(B)$ and $\rho_{xy}(B)$ of samples (a) EG1 and (b) EG2 for $0 < B < 9$ T.

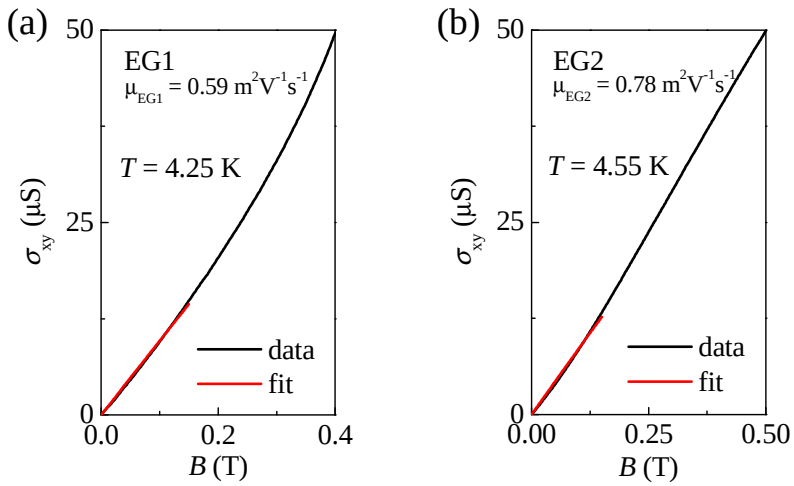

Figure S3 Determination of the mobility μ for samples (a) EG1 and (b) EG2 by fitting the measured σ_{xy} to $ne\mu^2B/(1+(\mu B)^2)$ over the range of $0 < B < 0.15$ T.

Weak localization and electron-electron interactions in our devices

In the weakly disordered regime, that is, the conductivity higher than $e^2/\pi h$, weak localization (WL) and electron-electron interaction (EEI) have significant contributions to the transport at low B in disordered graphene devices and may influence[11] the observed I-QH transitions.[12-16] The WL term modifies ρ_{xx} without affecting ρ_{xy}. The diffusive EEI has effects on both ρ_{xx} and ρ_{xy}. To investigate the observed I-QH transition, we have isolated the EEI contribution from the WL one following Ref. [17]. The EEI correction to the Drude conductivity[17] is given by

$$\delta\sigma_{xx}^{ee} = -K_{ee}G_0 \ln(\frac{\hbar}{k_B T\tau}), \quad (1)$$

where K_{ee} is an interaction parameter dependent on the type of sample and τ is the scattering time. This term gives a ln$T$ dependence to both σ_{xx} and to the Hall coefficient $R_H \equiv \delta\rho_{xy}(B, T)/\delta B$. The ln$T$ dependence of R_H is shown in Fig. S4 (a).

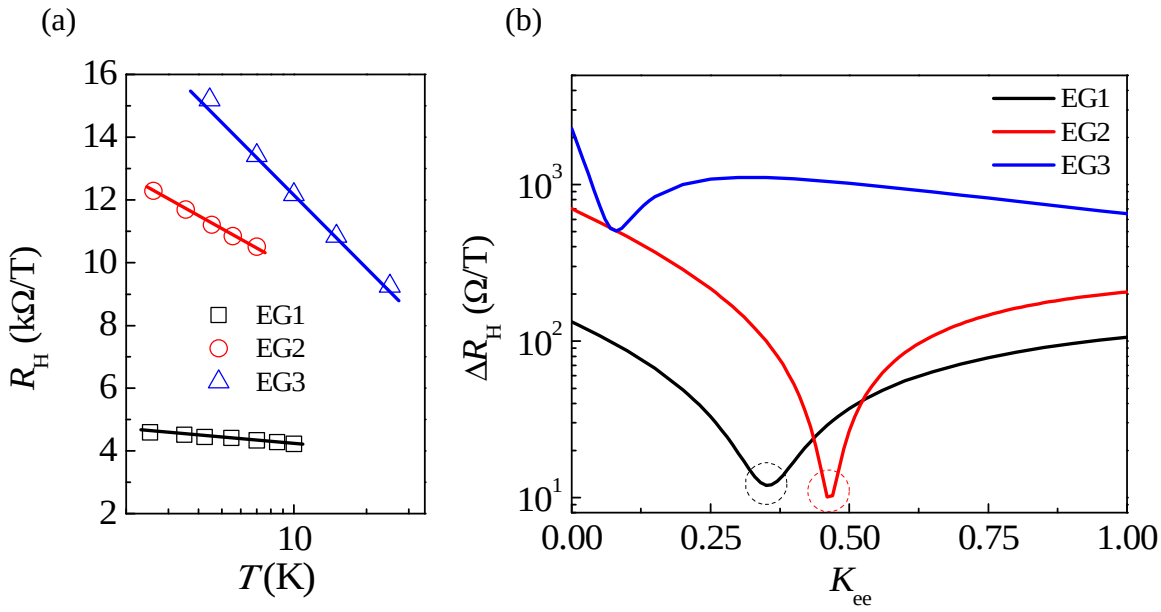

Fig. S4 (a) Uncorrected Hall slope $R_H \equiv \delta\rho_{xy}(B, T)/\delta B$ as a function of T. (b) Standard deviation of the corrected Hall slope at different T, $\Delta R_H = \sqrt{\frac{1}{N-1}\sum_i (R_H^i - \overline{R_H})^2}$ (where i runs over the measured temperature points), plotted against the interaction parameter K_{ee}. ΔR_H of the uncorrected data in (a) for each sample corresponds to $\triangle R_H(K_{ee} = 0)$ in (b).

According to Eq. (1), matrix inversion of the conductivity tensor shows that $\rho_{xx}(B,T)$ takes a parabolic form[18],

$$\rho_{xx} \approx \frac{1}{\sigma_D} - \frac{1}{\sigma_D^{\,2}}(1-\mu^2 B^2)\delta\sigma_{xx}^{ee}(T), \qquad (2)$$

for $\delta\sigma_{xx}^{ee} << \sigma_D$, where μ is the mobility, σ_D is the Drude conductivity and μ is the mobility. In addition, the EEI term gives a correction to the Hall coefficient $R_H \equiv \delta\rho_{xy}(B, T)/\delta B$ following $\delta R_H / R_H^0 = -2\delta\sigma_{ee}/\sigma_D$, where R_H^0 denotes the classical value of R_H [ref. 17]. The ln$T$ dependence of R_H is observed in Fig. S4(a), suggesting the influence of electron-electron interactions on the low-field insulating behavior.

Relevant to the data analysis, Eq. (2) indicates a T-independent point in ρ_{xx} at $\mu B = 1$. To clarify this its relation with the observed crossing issue, we remove the correction the contribution of EEI as described by Eq. (2) to ρ_{xx} at low B [ref. 18] and estimate the EEI strength following Ref. [17]. The correction $\delta\sigma_{xx}^{ee}$ described by Eq. (2) is subtracted from the measured σ_{xx} for with $0 \leq K_{ee} \leq 1$. By inverting the resulting conductivity tensor, we obtain a new corrected set of ρ_{xx} and ρ_{xy}. The optimum K_{ee} is identified when the standard deviation of the corrected R_H values at different T in Fig. S4(b) reaches its minimum. As shown in Figs. S5(a) and S5(c), for EG1 and EG2 the correction removal process renders the corrected ρ_{xy} insensitive to the change in T at low fields and the slope corresponds to R_H^0 without suffering from EEI. Most disordered device does not produce an optimum K_{ee} with reasonable confidence, and only a weak minimum (EG3) is obtained by this procedure. The T-independent points in $\rho_{xx}(B, T)$ survive in the corrected data for EG1 and EG2 and occur at only slightly lower crossing fields B_c^{ρ} after the correction [Figs. S5(a) and S5(b)]. The remaining T and B dependence of ρ_{xx} is attributed to WL effect (Supplementary Fig. S5), suggesting that the transition in EG1 and EG2 represents the crossover from WL to the $\nu = 2$ quantum Hall state. However, stronger disorder in EG3 whose low-T conductivity is lower than $e^2/\pi h$ makes the correction descriptions invalid.

Remove the corrections due to electron-electron interactions

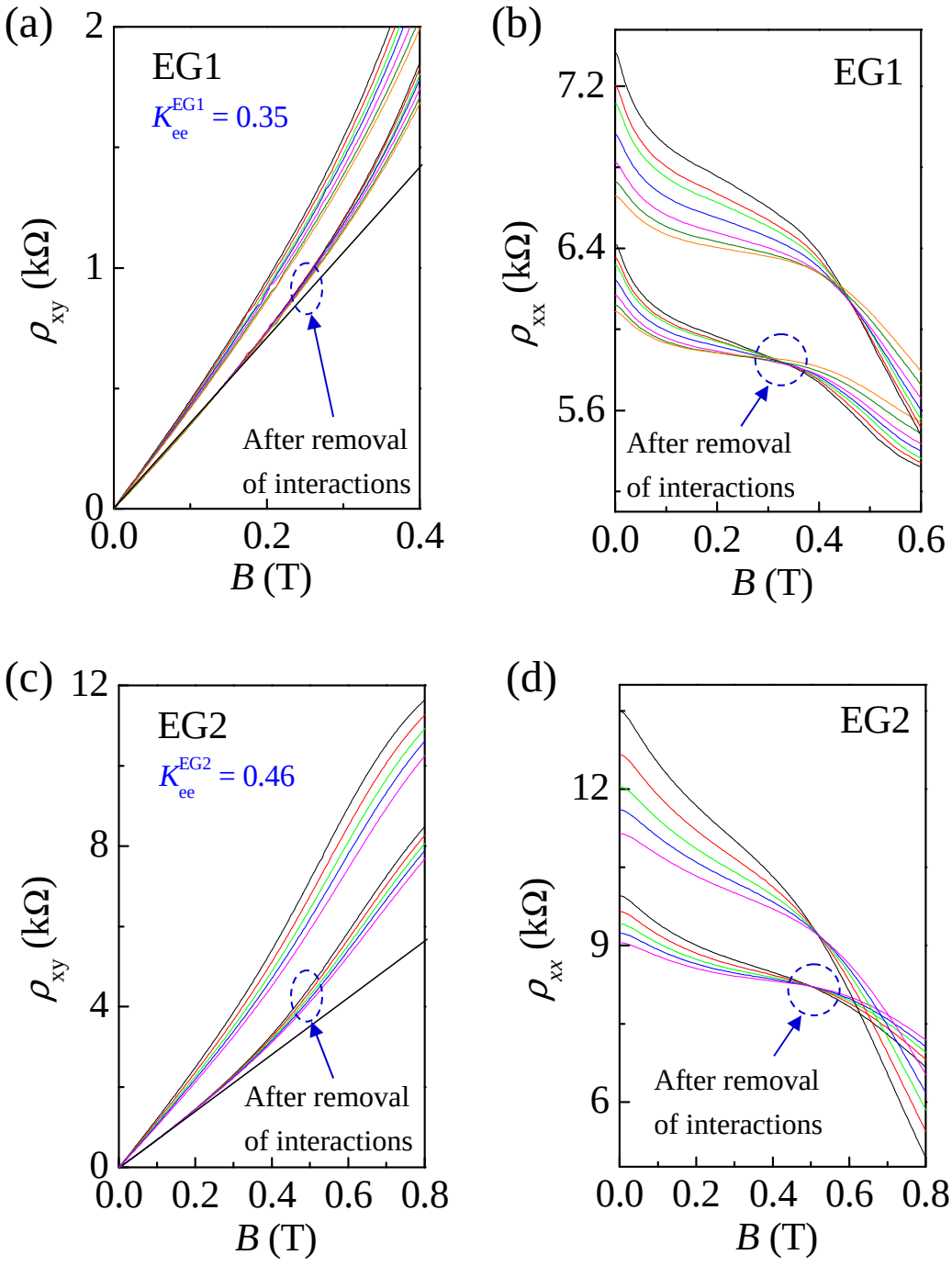

Fig. S5 Comparison of *T*-dependent resistivities for samples (a, b) EG1 and (c, d) EG2 before and after removal of interactions. The temperature ranges are the same as those given in the caption of Fig. 1.

Weak localization

Our experimental results can be fitted to the theoretical work of McCann *et al.*[19] as shown in Fig. S6 (a) and (b). We note that the WL effect contributes to a shift in σ_{xx} proportional to $\ln(\tau_\phi/\tau)$, where τ_ϕ is the phase relaxation time and approximately proportional to T^{-1} as shown in Fig. S6 (c); however, WL produces no contribution to Hall coefficient.

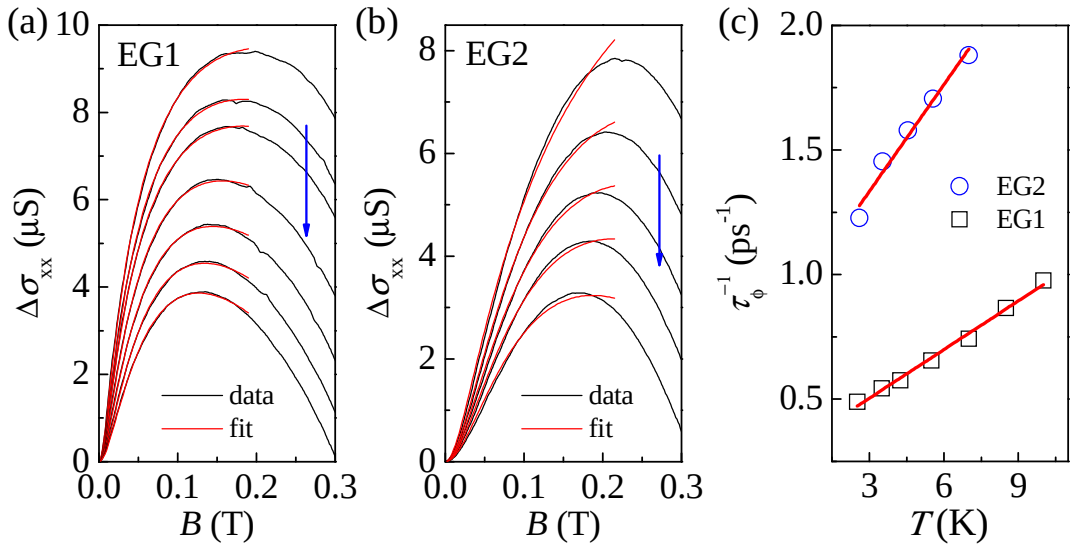

Figure S6 Fits of the measured $\Delta\sigma_{xx}(B) \equiv \sigma_{xx}(B) - \sigma_{xx}(B = 0)$ to the model developed by McCann *et al.* [19] for samples (a) EG1 and (b) EG2. The arrows indicate the temperature increase. (c) The decoherence rate τ_ϕ^{-1} obtained from the fits as a function of T.

Scaling of the Hall conductivity

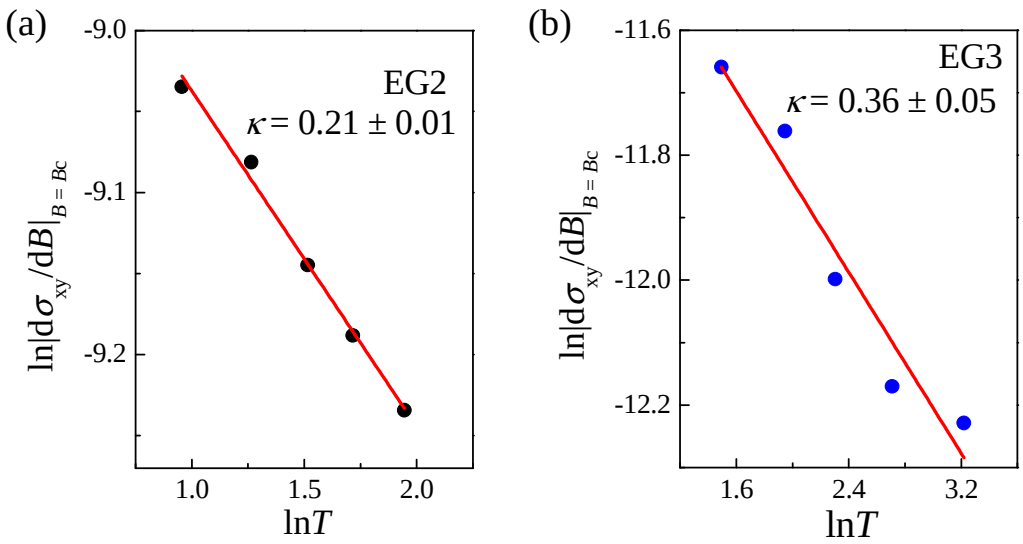

Figure S7 Fit of the slope of the transverse conductivity $d\sigma_{xy}/dB$ at the critical field B_c^{σ} to the power-law dependence on temperature T with an exponent κ for EG2 and EG3.

Table S1 Physical quantities of each EG sample.

Sample	Type	density (m^{-2})	K_{ee}	μ ($m^2V^{-1}s^{-1}$)	τ (fs)	Γ (meV)	μB_c^{ρ}
EG1	n	1.75×10^{15}	0.35	0.59	29	23	0.27
EG2	p	8.83×10^{14}	0.46	0.78	27	24	0.41
EG3	n	5.76×10^{14}	−	0.31	9	76	1.21

References

1. J. Ristein, S. Mammadov, and Th. Seyller, *Phys. Rev. Lett.* 2012, **108**, 246104.
2. D. B. Farmer *et al., Phys. Rev. B* 2011, **84**, 205417.
3. T. Shen *et al., J. Appl. Phys.* 2012, **111**, 013716.
4. S. Lara-Avila *et al., Adv. Mater.* 2011, **23**, 878-882.
5. C. Coletti *et al., Phys. Rev. B* 2010, **81**, 235401.
6. P. L. Levesque *et al., Nano Lett.* 2011, **11**, 132-137.
7. Y. Yang *et al., Small* 2015, **11**, 90-95.
8. S. Ryu *et al., Nano Lett.* 2010, **10**, 4944-4951.
9. Z. H. Ni *et al., J. Raman Spectros.* 2010, **41**, 479-483.
10. M. Hilke *et al., Nature* 1998, **395**, 675-677.
11. M. Y. Simmons *et al., Phys. Rev. Lett.* 2000, **84**, 2489-2492.
12. S. H. Song *et al., Phys. Rev. Lett.* 1997, **78**, 2200-2203.
13. H. W. Jiang *et al., Phys. Rev. Lett.* 1993, **71**, 1439-1442.
14. R. J. F. Hughes *et al., J. Phys.: Condens. Matter* 1994, **6**, 4763-4770.
15. T. Wang *et al., Phys. Rev. Lett*. 1994, **72**, 709-712.
16. E. Pallecchi *et al., Sci. Rep.* **3**, 1791 (2013).
17. K. E. J. Goh, M. Y. Simmons and A. R. Hamilton, *Phys. Rev. B* 2008, **77**, 235410.
18. G. M. Minkov *et al., Phys. Rev. B* 2003, **67**, 205306.
19. E. McCann *et al., Phys. Rev. Lett.* 2006, **97**, 146805.